Available online at www.sciencedirect.com
SCIENCE DIRECT®
International Journal of Heat and Mass Transfer 48 (2005) 4132–4149
International Journal of HEAT and MASS TRANSFER
www.elsevier.com/locate/ijhmt

A foam ablation model for lost foam casting of aluminum

M.R. Barone [1], D.A. Caulk *

Manufacturing Systems Research Laboratory, General Motors Research and Development Center, 30500 Mound Road, Warren, MI 48090, United States

Received 9 December 2004; received in revised form 18 February 2005

Abstract

A model is developed for heat transfer, polymer vaporization, and gas diffusion at the interface between the advancing liquid metal and the receding foam pattern during mold filling in lost foam casting of aluminum. Most of the pattern interior decomposes by ablation, but the boundary cells decompose by a collapse mechanism, which creates an undercut in the pattern next to the coating. By regulating how much of the pattern coating is exposed to gas diffusion, the undercut controls the overall filling speed of the metal through the mold. Computed values for the foam decomposition energy from this model compare very well with experimental data on foam pyrolysis, and predicted filling speeds are consistent with observations in published experiments. In addition, the model explains several unusual observations about mold filling that until now have not been understood.

Keywords: Lost foam; Casting; Ablation; Decomposition; Model

1. Introduction

1.1. Lost foam casting

First conceived by Maytag engineer Smith [1] in 1964, lost foam casting involves the novel use of an expendable pattern made of molded polymer foam. Sometimes patterns are glued together from two or more separately molded pieces when internal passages do not allow them to be molded as one. After the pattern is assembled, it is dipped in a water-based refractory slurry and allowed to dry. The coated pattern is then placed inside a steel flask, where it is surrounded with loose, dry sand. After the sand is compacted by vibration, liquid metal is poured directly into the pattern, which decomposes ahead of the advancing liquid metal as gas and liquid products from the receding foam diffuse through the coating and into the sand. The liquid metal eventually replaces all the volume occupied by the foam pattern before it solidifies [2].

As a process for making complex parts in high volume, lost foam casting has several important advantages. First, the molds for the foam patterns are relatively inexpensive and easy to make. Castings are free from parting lines, and draft angles can be reduced or even eliminated. Internal passages may be cast without cores, and many design features, such as pump housings and oil holes, can be cast directly into the part. Lost foam casting is also kinder to the environment than traditional green sand casting because the sand can be cleaned and reused. Although lost foam casting is used

* Corresponding author. Tel.: +1 586 986 0453; fax: +1 586 986 0574.
E-mail address: david.a.caulk@gm.com (D.A. Caulk).
[1] Retired from General Motors in December, 2002.

0017-9310/$ - see front matter © 2005 Elsevier Ltd. All rights reserved.
doi:10.1016/j.ijheatmasstransfer.2005.03.031

Nomenclature

a	coefficient in Arrhenius expression for vaporization rate, kg/s m^2
c_A	specific heat of the air in the decomposition layer, J/kg K
c_L	specific heat of the polymer liquid in the decomposition layer, J/kg K
c_S	specific heat of the solid polymer in the foam, J/kg K
c_V	specific heat of the polymer vapor in the decomposition layer, J/kg K
d	pattern thickness, m
d_C	coating thickness, m
E	activation energy in Arrhenius expression for vaporization rate, J/mole
H_D	heat of degradation per unit mass for the polymer in the foam, J/kg
H_M	latent heat of fusion per unit mass for the polymer in the foam, J/kg
H_V	heat of vaporization per unit mass for the polymer in the foam, J/kg
k_D	bulk thermal conductivity of the liquid foam, W/m K
K_0	zeroth-order modified Bessel function of the second kind
l_C	length of exposed coating open to gas diffusion, m
l_D	thickness of the decomposition layer, m
m_D	normal mass flux of liquid foam in decomposition layer, kg/s m^2
M_V	mass-average molecular weight of the polymer vapor in the decomposition layer, kg/mole
n	exponent in Arrhenius expression for vaporization rate
p_0	atmospheric pressure, Pa
p_C	pressure on the inside surface of the coating, Pa
p_D	pressure in the decomposition layer, Pa
p_M	pressure in the liquid metal, Pa
p_S	pressure on the outside surface of the coating, Pa
P	Peclet number in the coating undercut
q_M	heat flux from the surface of the liquid metal into the decomposition layer, W/m^2
r_V	mass rate of polymer vaporization per unit area at the metal surface, kg/s m^2
R	universal gas constant
u	mold filling speed, m/s
v_G	filter velocity of the gas diffusing through the coating, m/s
x	Cartesian coordinate, m
x_V	mass fraction of polymer liquid vaporized in the decomposition layer
y	Cartesian coordinate, m

Greek symbols

β	nondimensional number in analysis of gas diffusion through the sand
δ	width of the coating undercut, m
δ_0	nominal cell size of the expanded foam beads, m
δ_D	maximum width of the coating undercut, m
δ_L	thickness of residual polymer liquid that accumulates along the undercut, m
ε_A	internal energy per unit mass of the air in the decomposition layer, J/kg
ε_C	energy per unit mass required to collapse the foam, J/kg
ε_D	internal energy per unit mass of the liquid foam in the decomposition layer, J/kg
ε_L	internal energy per unit mass of the polymer liquid in the decomposition layer, J/kg
ε_P	energy per unit mass required to "melt" the foam, J/kg
ε_{PD}	energy per unit mass required to decompose the foam pattern, J/kg
ε_V	internal energy per unit mass of the polymer vapor in the decomposition layer, J/kg
θ	temperature of the liquid foam, K
θ_0	initial temperature of the pattern and sand, K
θ_C	collapse temperature of the foam, K
θ_D	average temperature in the decomposition layer, K
θ_L	average temperature of the residual polymer liquid along the undercut, K
θ_M	temperature on the metal surface, K
θ_P	nominal melting temperature of the foam pattern, K
κ_C	gas permeability of the coating, m^2
κ_S	gas permeability of the sand, m^2
λ_D	Peclet number in the decomposition layer
λ_U	modified Peclet number in the coating undercut
μ_G	viscosity of the gas escaping through the coating, Pa s
ρ_A	partial density of the air in the decomposition layer, kg/m^3
ρ_A^0	density of the air in the pattern at its initial pressure and temperature, kg/m^3
ρ_B	boundary density of the foam pattern, kg/m^3
ρ_D	average density of the liquid foam in the decomposition layer, kg/m^3

ρ_F	partial density of the polymer in the foam, kg/m^3	ρ_P	total density of the foam pattern, kg/m^3
ρ_G	average density of the gas in the undercut, kg/m^3	ρ_S	density of the polymer in the foam, kg/m^3
ρ_L	partial density of the polymer liquid in the decomposition layer, kg/m^3	ρ_V	partial density of the polymer vapor in the decomposition layer, kg/m^3
		φ	volume fraction of air in the foam
		φ_S	porosity of the sand

to cast a variety of alloys, the present paper is restricted to aluminum.

One of the important technical challenges in lost foam casting is to understand the connection between the mechanics of foam decomposition during mold filling and the formation of excessive internal porosity or folds (a pair of poorly fused metal surfaces contaminated by oxide and/or carbon residue) in the final cast product [3]. Such anomalies can occur when products of foam decomposition do not fully escape from the mold cavity before the casting solidifies. If such physical understanding can be embodied in a mathematical model of foam decomposition and mold filling, it should be possible to predict conditions that lead to such fill-related anomalies and then correct (or at least reduce) them by redesigning the product or reengineering the process before any tooling is made. This should help to eliminate much of the costly trial and error that is now so prevalent during process development in lost foam casting.

1.2. The mold filling problem

Unlike traditional casting processes where metal is poured directly into an empty mold cavity, the movement of liquid metal through a lost foam mold is determined more by the rate of foam decomposition ahead of the flow front than it is by the dynamics of metal flow behind it. The metal simply moves into the mold volume originally occupied by the foam pattern as fast as the foam decomposes and the products of that decomposition are pushed out of the way. Up to now, most attempts at modeling the mold filling process in lost foam casting have replaced the complex mechanics of foam decomposition by a simplified empirical boundary condition at the metal/foam interface, and then solved the metal flow problem by more-or-less conventional means. Tsai and Chen [4], Hirt and Barkhudarov [5], and Liu et al. [6] assign a constant heat transfer coefficient to the interface between the metal and the foam, and then compute a flow-front velocity by relating the resulting heat flux to a constant foam decomposition energy. Wang et al. [7] and Gurdogan et al. [8] both assume that the flow-front velocity is a linear function of the metal temperature and pressure, with empirical coefficients obtained from one-dimensional filling experiments. Shivkumar [9] simply assigns the metal velocity directly, again based on one-dimensional filling data. Even if one of these approaches were successful in describing the flow of liquid metal in the mold cavity, though, it would still be unable to shed much light on the physical mechanisms that cause fill-related porosity or folds simply because the mechanics of foam decomposition are obscured by empiricism. To truly get at the cause of such anomalies, foam decomposition must be modeled as a separate physical process.

1.3. Foam decomposition

As more and more experimental observations have been made of mold filling in lost foam casting, it has become increasingly clear that depending on the local conditions inside the mold, the foam can decompose by more than one physical mechanism [10]. This paper is concerned with just one such mechanism—one we call *contact mode*. In contact mode the liquid metal makes direct contact with the foam pattern, decomposing it primarily by ablation. Contact mode is by far the most prevalent mode of foam decomposition in lost foam casting, and the one—at least for low melting point alloys—that occurs before any other sets in.

In this paper, we construct a model for heat conduction in the narrow layer separating the liquid metal and the foam pattern, including the convection of liquid foam out of the receding pattern and partial vaporization of the polymer liquid at the metal surface. We also propose a separate collapse mechanism for the foam cells on the boundary of the pattern, which leads to a new concept we call the *coating undercut*. The rate of propagation of the coating undercut along the boundary of the pattern determines how fast the mold fills. The calculated filling speeds predicted by this model not only compare very well with measurements for aluminum alloys, but they also help to explain the reasons for several unusual experimental observations that until now have not been clearly understood.

2. The decomposition layer

2.1. Structure and composition

Consider liquid metal in direct contact with a polymer foam pattern, separated by only a narrow layer

containing liquid and gas from the decomposing foam. The foam decomposes at a steady velocity u, as depicted in Fig. 1, with the decomposition products escaping laterally along the layer towards the coating on each side. We assume the liquid metal has a locally planar front with the origin of coordinates moving with the metal and the x-axis pointing into the foam. We neglect all temperature gradients parallel to the surface of the metal compared with the much steeper gradients directed towards the foam. Let θ_M denote the uniform temperature on the surface of the metal and θ_0 the initial temperature of the pattern. Even though most foam materials are glassy polymers without a well-defined melting temperature, they usually soften and then liquefy over a fairly narrow temperature range [11]. Hence we assume the foam becomes a liquid at the plane $x = l_D$, where the pattern temperature reaches a nominal melting temperature designated by θ_P. The interval $0 < x < l_D$ between the liquid metal and the solid foam is called the *decomposition layer*.

Although the foam pattern may contain residual blowing agents left over from the molding process, we assume that by the time the casting is poured the volume of such gases is negligible, so that the foam is made up entirely of solid polymer and air. Let φ denote the volume fraction of air in the foam, ρ_S the mass density of the polymer material, and ρ_A^0 the density of air at the initial pattern temperature θ_0 and atmospheric pressure p_0. Then the total density ρ_P of the foam pattern is given by

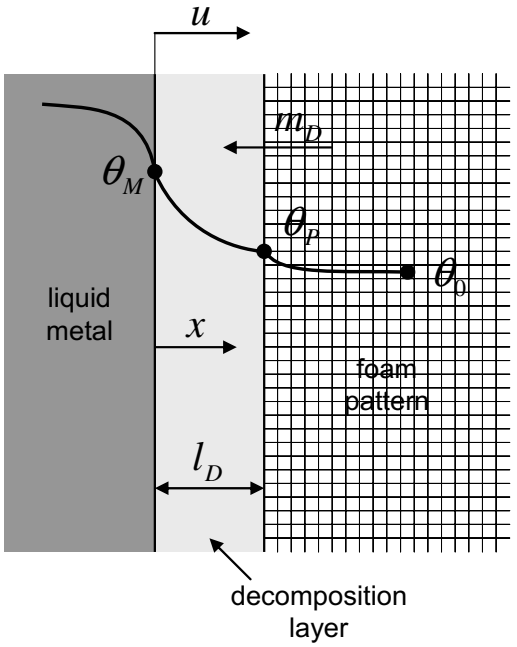

Fig. 1. Schematic illustration of the decomposition layer between the liquid metal and the receding foam.

$$\rho_P = \varphi\rho_A^0 + (1-\varphi)\rho_S = \varphi\rho_A^0 + \rho_F, \tag{2.1}$$

where $\rho_F = (1-\varphi)\rho_S$ is the partial density of the polymer in the foam.

During controlled foam pyrolysis experiments in which a foam bar was passed through an electrically heated metal strip at velocities typical of mold filling speeds in lost foam casting, Molibog and Littleton [12] observed "frothy liquid" squeezing out between the metal strip and the impinging foam. (Their experiment is described in more detail later in this section.) Based on these observations, we assume that the gas and liquid in the decomposition layer do not separate into distinct regions, but instead combine to form a homogeneous *liquid foam*. To minimize surface energy, the small liquid fraction in this foam (typically less than 1%) collects in *Plateau borders* at junctions of three or more cells in the foam structure [13]. As these slender liquid filaments contact the surface of the liquid metal, they vaporize, creating additional polymer vapor that combines with the gas already in the decomposition layer.

Let x_V denote the mass fraction of the original polymer that vaporizes as the liquid foam passes through the decomposition layer on its way to the coating. Molibog and Littleton [14] observed very little degradation in the residual liquid they collected in their foam pyrolysis experiments, and so it is likely that the liquid polymer undergoes most of its depolymerization just before it vaporizes. For simplicity we assume that both reactions occur simultaneously at the metal surface $x = 0$, and that the rate of vaporization r_V per unit area on that surface is specified by an Arrhenius relationship in the form

$$r_V = r_V(\theta_M, x_V) = a\exp(-E/R\theta_M)(1-x_V)^n, \tag{2.2}$$

where R denotes the universal gas constant and the values of a, E, and n depend on the foam material. The constant E, called the *activation energy*, measures the reaction's sensitivity to temperature. As the metal temperature increases, the rate of vaporization also increases. The exponent n measures the sensitivity of vaporization rate to the amount of available liquid. As x_V increases, the liquid foam contains less liquid and the rate of vaporization decreases. From the definition of x_V it follows that

$$x_V\rho_F u = r_V(\theta_M, x_V). \tag{2.3}$$

Unless otherwise indicated, all temperatures and pressures in this paper are taken to be absolute quantities.

Let p_D denote the pressure in the decomposition layer, which we assume is independent of x. Let M_V denote the mass-average molecular weight of the polymer vapor and θ_D the average temperature of the liquid foam. Then if we assume that the air and polymer vapor behave as ideal gases, it is not difficult to show that the average mass density ρ_D in the decomposition layer is given by

$$\rho_D = \frac{\rho_P}{(1-x_V)(1-\varphi) + x_V\rho_F\dfrac{R\theta_D}{p_D M_V} + \varphi\dfrac{p_0\theta_D}{p_D\theta_0}}. \tag{2.4}$$

Because of the small volume fraction of liquid, the first term in the denominator of (2.4) is usually negligible compared with the other two.

Now let ρ_A, ρ_V, and ρ_L denote the partial densities of air, polymer vapor, and polymer liquid, respectively, in the liquid foam. Then since the mass fractions of air and polymer in the decomposition layer must be the same as those in the solid foam, we have

$$\begin{aligned} \rho_A/\rho_D &= \varphi\rho_A^0/\rho_P, \\ \rho_V/\rho_D &= x_V\rho_F/\rho_P, \\ \rho_L/\rho_D &= (1-x_V)\rho_F/\rho_P. \end{aligned} \tag{2.5}$$

Let ε_A, ε_V, and ε_L denote the internal energies per unit mass of the air, polymer vapor, and polymer liquid, respectively. Then the average internal energy ε_D in the decomposition layer is given by

$$\rho_D\varepsilon_D = \rho_A\varepsilon_A + \rho_V\varepsilon_V + \rho_L\varepsilon_L. \tag{2.6}$$

Further, let c_A, c_V, and c_L denote the corresponding specific heats per unit mass of the air, polymer vapor, and polymer liquid, respectively. We assume that each is approximately constant over the temperature range in the decomposition layer. Then the average specific heat c_D in the decomposition layer is given by

$$\rho_D c_D = \rho_A c_A + \rho_V c_V + \rho_L c_L. \tag{2.7}$$

With the help of (2.5), the two expressions (2.6) and (2.7), may be written in the more convenient forms

$$\rho_P\varepsilon_D = \varphi\rho_A^0\varepsilon_A + x_V\rho_F\varepsilon_V + (1-x_V)\rho_F\varepsilon_L, \tag{2.8}$$

$$\rho_P c_D = \varphi\rho_A^0 c_A + x_V\rho_F c_V + (1-x_V)\rho_F c_L. \tag{2.9}$$

For later reference we also define the energy per unit mass ε_P required to heat the foam from its initial temperature θ_0 to its "melting" temperature θ_P. If we let c_S denote the specific heat per unit mass of the solid polymer and H_M its latent heat of fusion, then it follows that

$$\rho_P\varepsilon_P = (\varphi\rho_A^0 c_A + \rho_F c_S)(\theta_P - \theta_0) + \rho_F H_M. \tag{2.10}$$

Since most foam materials are amorphous polymers, their latent heat of fusion is usually negligible. In particular, both Tseng and Askeland [15] and Mehta et al. [11] detected no significant melting energy for polystyrene foam.

2.2. Energy balance

We assume that as the liquid metal advances through the foam, all material originally in the foam enters the decomposition layer at $x = l_D$ and then exits laterally towards the coating. In other words, no air or polymer vapor escapes ahead of the metal through any open porosity that may be present in foam. This means that for a steady metal velocity u, the normal mass flux m_D entering the decomposition layer at $x = l_D$ is simply $\rho_P u$ (Fig. 1). The lateral movement of this material towards the coating causes m_D to decrease with x until it vanishes entirely at the metal surface $x = 0$. For simplicity, we assume that m_D is linear in x, so that

$$m_D = \rho_P u x/l_D. \tag{2.11}$$

Let k_D denote the bulk thermal conductivity of the liquid foam in the decomposition layer and let $\theta(x)$ designate its temperature distribution. Then the energy balance equation in the decomposition layer is given by

$$k_D\frac{\partial^2\theta}{\partial x^2} + \left(\frac{\rho_P c_D u x}{l_D}\right)\frac{\partial\theta}{\partial x} = 0, \quad 0 < x < l_D. \tag{2.12}$$

There is no explicit source term in (2.12) because of the earlier assumption that all polymer degradation and vaporization takes place at the metal surface $x = 0$. There is also no lateral convection term because the temperature gradients parallel to the metal surface are negligible. The appropriate boundary conditions are

$$\theta(0) = \theta_M, \quad \theta(l_D) = \theta_P, \quad -k_D\frac{\partial\theta}{\partial x}(l_D) = \rho_P\varepsilon_P u. \tag{2.13}$$

The last of these ensures that the heat flux at $x = l_D$ is sufficient to melt the foam at the prescribed rate. The solution of (2.12) that satisfies the first two conditions in (2.13) is

$$\theta = \theta_M - \frac{\operatorname{erf}(\lambda_D x/l_D)}{\operatorname{erf}(\lambda_D)}(\theta_M - \theta_P), \tag{2.14}$$

where λ_D is a Peclet number for the decomposition layer defined by

$$\lambda_D^2 = \frac{\rho_P c_D u l_D}{2k_D}. \tag{2.15}$$

Together with (2.14), the third condition in (2.13) provides an independent equation for determining λ_D, namely,

$$\theta_M - \theta_P = \pi^{1/2}(\varepsilon_P/c_D)\lambda_D e^{\lambda_D^2}\operatorname{erf}(\lambda_D). \tag{2.16}$$

The average temperature θ_D in the decomposition layer may be calculated by integrating (2.14) across the decomposition layer. With the help of (2.16), the result is

$$\theta_D = \frac{1}{l_D}\int_0^{l_D}\theta(x)\,dx = \theta_P + (\varepsilon_P/c_D)(e^{\lambda_D^2} - 1). \tag{2.17}$$

Since both θ_M and θ_D depend solely on the Peclet number λ_D, it is possible, at least in principle, to eliminate λ_D between (2.16) and (2.17) and express θ_D as a function of the metal temperature alone. This means that the average temperature in the decomposition layer, like the Peclet number, is independent of the filling speed u.

The total heat flux q_M from the surface of the liquid metal is

$$q_M = -k_D \frac{\partial \theta}{\partial x}(0) + r_V(H_V + H_D)$$
$$= \rho_P \varepsilon_P u e^{\lambda_D^2} + x_V \rho_F u (H_V + H_D), \quad (2.18)$$

where H_D and H_V denote the heats of degradation and vaporization per unit mass of the polymer, respectively. With the help of (2.17), this expression may be written in the alternative form

$$\varepsilon_{PD} = \frac{q_M}{\rho_P u} = \varepsilon_P + c_D(\theta_D - \theta_P) + x_V \frac{\rho_F}{\rho_P}(H_V + H_D). \quad (2.19)$$

The quantity ε_{PD}, the total energy required to remove the foam from the path of the liquid metal, is called the *pattern decomposition energy*. The first term in (2.19) represents the energy required to melt the foam. The next represents the energy required to heat the liquid foam to the average temperature of the decomposition layer. The last term is the energy required to degrade and vaporize the portion of the polymer liquid that comes into contact with the surface of the liquid metal.

2.3. Selected results for polystyrene foam

Before developing the foam decomposition model any further, we pause and consider how well the results obtained so far agree with available experimental data for expanded polystyrene foam. Molibog and Littleton [12,14] developed a foam pyrolysis apparatus to simulate the interaction between a foam pattern and liquid metal in lost foam casting. The apparatus pushes a long foam bar through an electrically heated metal strip either at a constant velocity or with a constant applied force. The metal strip is maintained at a constant temperature by regulating its power input. After the foam bar is pyrolyzed by the heated metal strip, the mass of residual foam and congealed liquid is subtracted from the mass of the original bar to determine the amount of gas generated as the foam decomposes. In this way it is possible to measure the gas fraction x_V and then calculate the rate of vaporization r_V from (2.3).

Molibog and Littleton [14] pyrolyzed three lost foam grade polystyrene foam materials at nominal velocities of 1, 3, and 4.5 cm/s. Fig. 2 shows a plot of gas fraction measurements (open symbols) as a function of heater temperature for one of those materials (StyroChem T170B with a nominal density of 25 kg/m^3) at all three speeds. Each open symbol on these graphs represents a measurement from a single foam bar. The corresponding rates of vaporization calculated from (2.3) are plotted in Fig. 3.

To determine the three kinetic parameters in (2.2) from this data, we first take the logarithm of (2.2) and perform linear regression analysis on the data in Fig. 3 to determine values for the three constants that give

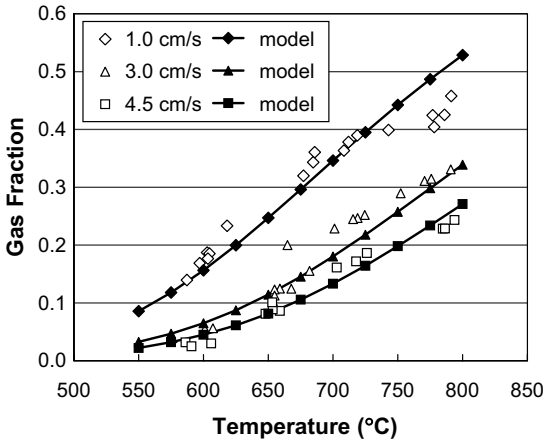

Fig. 2. Mass fraction of gas generated during foam pyrolysis of expanded polystyrene foam. Open symbols represent Molibog and Littleton's [14] experimental data. Solid lines and symbols are derived from (2.2) and (2.3) using the constants in (2.20).

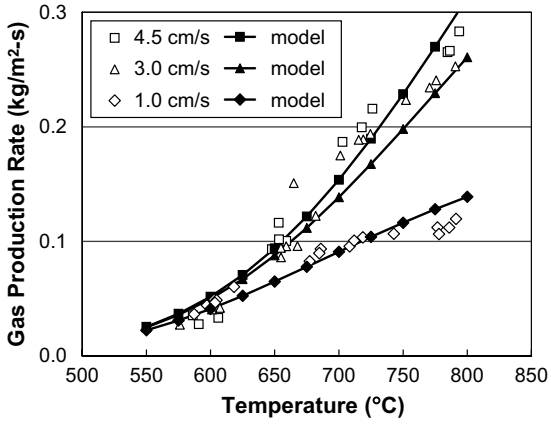

Fig. 3. Gas production rate during foam pyrolysis of expanded polystyrene foam. Open symbols represent Molibog and Littleton's [14] experimental data. Solid lines and symbols are derived from the vaporization equation (2.2) using the constants in (2.20).

the best fit to the empirical equation (2.2). The results are

$$a = 13{,}000\ \text{kg/m}^2\ \text{s}, \quad E = 90\ \text{kJ/mole}, \quad n = 1.9. \quad (2.20)$$

The activation energy of 90 kJ/mole is consistent with values reported by Sands and Shivkumar [16] for a similar material. After substituting these constants into (2.2) and solving the mass balance equation (2.3), we can determine the gas fraction x_V and the average gas generation rate r_V for given values of temperature and speed. These calculated results are also plotted in Figs. 2 and 3.

The discrepancies between the empirical relationship (2.2) and the experimental data are comparable with the variation in the data.

Table 1 lists typical properties for polystyrene foam. We assume that the polymer degradation is nearly complete at vaporization, so that the molecular weight of the gas is that of styrene monomer. With these properties, we can solve (2.16) for λ_D and (2.3) for x_V for given values of the filling speed and metal temperature and then substitute these two results into (2.18) to calculate the heat flux. The results are plotted in Fig. 4, together with the corresponding measurements from Molibog and Littleton's [14] experiments. Since these measurements are independent of the gas fraction data recorded earlier, they serve as a check on the validity of the model. The predicted fluxes fall short of the measurements by about 10%. This may be due to some additional heating of the foam as it passed over the top and bottom edges of the metal heater, something that was not included in the analysis.

Fig. 5 shows how the Peclet number λ_D varies as a function of temperature in these experiments. It is interesting to note that λ_D is nearly constant over the entire temperature range. According to (2.15), then, the thickness of the decomposition layer l_D varies almost inversely with the filling speed u.

Fig. 6 displays the temperature solution (2.14) corresponding to $\theta_M = 650$ °C, a typical value for aluminum alloys. The concave shape of the curve is caused by the convection of the cooler decomposition products from the decomposing pattern towards the hotter liquid

Table 1
Material properties of polystyrene foam

Property	Symbol	Value	Unit
Nominal foam density	ρ_F	25	kg/m^3
Foam boundary density	ρ_B	50	kg/m^3
Polymer density	ρ_S	800	kg/m^3
Nominal cell size	δ_0	50	μm
Thermal conductivity	k_D	0.04	W/m K
Melting temperature	θ_P	150	°C
Melting energy	H_M	0	J/g
Degradation energy	H_D	670	J/g
Vaporization energy	H_V	360	J/g
Specific heat of solid	c_S	1.5	J/g K
Specific heat of liquid	c_L	2.2	J/g K
Specific heat of vapor	c_V	2.2	J/g K
Molecular weight of vapor	M_V	104	g/mole
Viscosity of gas	μ_G	2×10^{-5}	Pa s

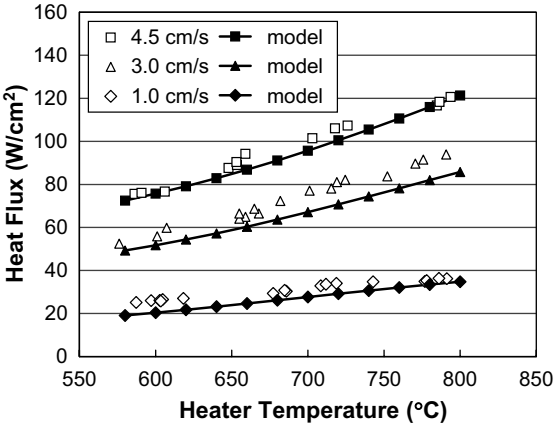

Fig. 4. Heat flux during foam pyrolysis of expanded polystyrene foam. Open symbols represent Molibog and Littleton's [14] experimental data. Solid lines and symbols are derived from (2.18) using the properties in (2.20) and Table 1.

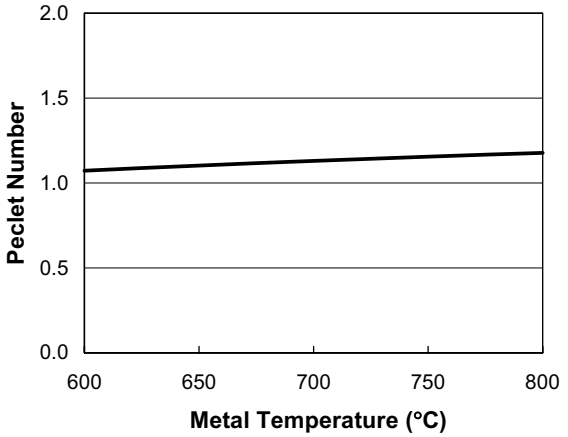

Fig. 5. Variation of the Peclet number λ_D in the decomposition layer over a typical range of metal temperatures for molten aluminum.

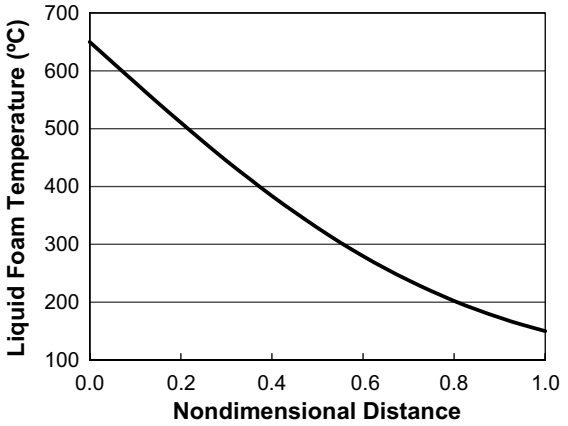

Fig. 6. Temperature variation through the decomposition layer for a polystyrene pattern (Table 1) and a metal temperature of 650 °C.

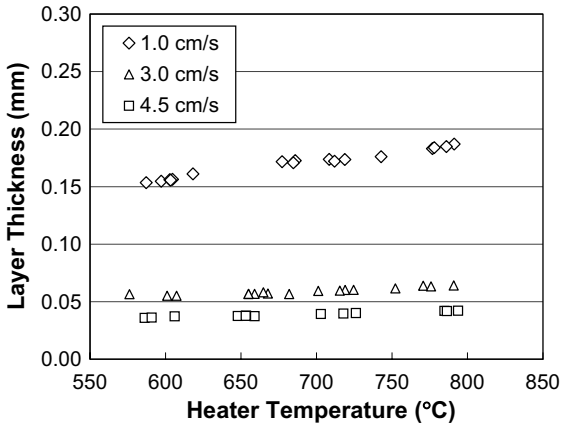

Fig. 7. Calculated thickness of the decomposition layer as a function of metal temperature for three different filling speeds.

metal. In general, convection depresses the average decomposition layer temperature (2.17) by about 50 °C.

Since the velocity u is a known quantity in these experiments, it is possible to use (2.9) and (2.15), together with computed values of λ_D and measured values of x_V, to calculate the thickness of the decomposition layer. Fig. 7 plots the results as a function of temperature and speed. According to these calculations, the decomposition layer is about 150 μm thick at typical filling speeds (1–2 cm/s), which is certainly too thin to observe with the naked eye. This is consistent with Butler and Pope's [17] early observations of mold filling through a glass window, where they reported no discernable gap between the liquid metal and the unmelted foam. Later experiments by Tseng and Askeland [18] and Walling and Dantzig [19] revealed the same thing. Interestingly, the thickness of the decomposition layer is the only result so far that is affected by the conductivity k_D of the liquid foam.

2.4. Viscous resistance

Although up to now we have not considered any lateral variation of the pressure p_D in the decomposition layer, a finite pressure gradient must of course exist to overcome viscous resistance of the liquid foam as it flows towards the coating in the narrow gap between the liquid metal and the unmelted foam. This gradient diminishes the available pressure at the coating for driving gas diffusion. In their foam pyrolysis experiments, Molibog and Littleton [14] measured the load exerted on the end of the foam bar as a function of speed and heater temperature. After correcting for the friction and other incidental forces unrelated to contact with the heater, they converted this load to an average pressure exerted by the foam bar on the surface of the heated metal strip. Measured pressures were less than 1 kPa for a heater width of 1 cm and a foam speed of 1 cm/s. This corresponds to about 4 cm of aluminum head height, which is less than 10% of the typical metal pressures at the flow front and comparable with the normal fluctuation in the metal head as it is poured. Although it is possible to extend the model to include the viscous resistance of the foam, it turns out to have a second-order effect on the main results, and so for now we simply neglect it.

Regardless of how small the viscous resistance of the liquid foam, the only way the metal has to support the required pressure gradient is by changing the shape of its flow front so that surface tension produces a nonuniform pressure in the decomposition layer. In extreme cases, this can result in an entirely different mechanism of foam decomposition. Such behavior, however, is outside the scope of the present paper. In what follows, we neglect surface tension entirely and assume that the pressure p_D in the decomposition layer is equal to the local pressure p_M in the liquid metal.

3. Gas diffusion

3.1. Coating

Since the coating and the sand are both permeable to gas diffusion, the pressure from the liquid metal inside the mold cavity forces the gas generated by the decomposing foam through the porous coating and into the surrounding sand. In principle, the escaping gas encounters diffusive resistance in both the coating and the sand. The rate at which the coating and sand allow gas to escape from the mold cavity determines how fast the mold fills. We consider the coating first.

Consider a length l_C of exposed coating near the flow front that is open to gas diffusion, bounded in front by the point where unmelted foam still adheres to the coating and behind by the point where either liquid metal or liquid polystyrene blocks the surface of the coating to gas diffusion. In quasi-steady mold filling, this open section of coating moves with the flow front at velocity u. Consider Cartesian coordinates moving with the flow front, such that the origin is centered in the section of exposed coating and the y-axis points into the sand (Fig. 8). We assume that relative to these coordinates the pressure in both the coating and the sand is independent of time. Let d_C represent the coating thickness and κ_C its gas permeability. Table 2 lists typical properties for coatings used in aluminum casting. Although many different types of coatings are used in aluminum casting, most of those in current use have properties very similar those in Table 2.

We assume that the mixture of air and polymer vapor has a constant viscosity μ_G and that it behaves as an ideal gas. If we further assume that $l_C \gg d_C$ (which

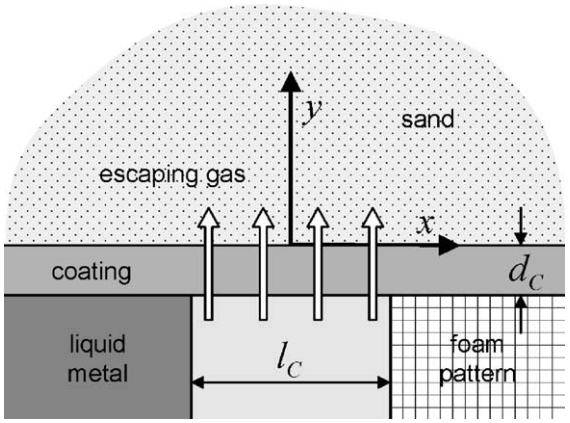

Fig. 8. Local geometry and coordinates for gas diffusion through the coating and into the sand.

Table 2
Material properties for the sand and coating

	Property	Symbol	Value	Unit
Sand	Permeability	κ_S	100	μm^2
	Porosity	φ_S	0.4	
Coating	Permeability	κ_C	0.02	μm^2
	Thickness	d_C	0.2	mm

should become evident in the next section), then the gas diffusion is predominately one-dimensional. At the relatively slow rates of diffusion found in aluminum casting, Darcy's law is valid, and so the filter velocity v_G of the escaping gas is given by [20]

$$v_G = \frac{\kappa_C}{\mu_G d_C}\frac{p_C^2 - p_S^2}{2p_C}, \tag{3.1}$$

where p_C is the gas pressure on the inside of the coating and p_S is the pressure in the sand just outside the coating. This equation relates the rate of gas diffusion to the pressure drop across the coating. To determine p_S, we must consider how gas disperses in the sand.

3.2. Sand

We assume that the sand extends indefinitely in all directions from the pattern and let p_0 denote the uniform pressure in the sand at infinity. Let κ_S denote the permeability of the sand and φ_S its porosity. Table 2 lists typical properties for silica sand. Just as in the coating, we assume that the gas is ideal and that it diffuses through the sand according to Darcy's law. The equation governing the gas pressure in the sand is [20]

$$\frac{\partial^2(p^2)}{\partial x^2} + \frac{\partial^2(p^2)}{\partial y^2} = \frac{2\varphi_S\mu_G}{\kappa_S}\left(u\frac{\partial p}{\partial x}\right). \tag{3.2}$$

If $p_S - p_0 \ll p_0$, then (3.2) may be approximated by

$$\frac{\partial^2(p^2)}{\partial x^2} + \frac{\partial^2(p^2)}{\partial y^2} = \frac{\varphi_S\mu_G u}{\kappa_S p_0}\frac{\partial(p^2)}{\partial x}. \tag{3.3}$$

From Darcy's law, the filter velocity on the surface of the sand is given by

$$-\frac{\kappa_S}{\mu_G}\frac{\partial p}{\partial y}(x,0) = v_G, \quad -\frac{1}{2}l_C < x < \frac{1}{2}l_C, \tag{3.4}$$

which, for small changes in pressure, may be approximated by

$$-\frac{\kappa_S}{2\mu_G p_0}\frac{\partial(p^2)}{\partial y}(x,0) = v_G, \quad -\frac{1}{2}l_C < x < \frac{1}{2}l_C. \tag{3.5}$$

Everywhere else on $y = 0$ the pressure gradient vanishes.

The problem stated in (3.3) and (3.5) is completely analogous to transient heat conduction from a uniform heat source on a moving strip in an infinite medium, as long as the square of the pressure is identified with temperature. The solution for the surface pressure, from Carslaw and Jaeger [21], is given by

$$p_S^2 - p_0^2 = \frac{4v_G p_0^2}{\pi\varphi_S u}\int_{\beta(2x/l_C-1)}^{\beta(2x/l_C+1)} e^{\xi}K_0(|\xi|)\,d\xi, \tag{3.6}$$

where K_0 is the zeroth-order modified Bessel function of the second kind and

$$\beta = \frac{\varphi_S\mu_G u l_C}{4\kappa_S p_0}. \tag{3.7}$$

For all cases of practical interest $\beta \ll 1$, so that the surface pressure reaches its maximum value very near $x = 0$. Therefore to an excellent approximation

$$\begin{aligned} p_S^2 - p_0^2 &\leqslant \frac{4v_G p_0^2}{\pi\varphi_S u}\int_{-\beta}^{\beta} e^{\xi}K_0(|\xi|)\,d\xi \\ &= \frac{4v_G p_0^2}{\pi\varphi_S u}\beta(e^{\beta} + e^{-\beta})K_0(\beta) \\ &\approx -\frac{8v_G p_0^2}{\pi\varphi_S u}\beta\ln(\beta). \end{aligned} \tag{3.8}$$

Dividing this expression by (3.1), we can estimate the ratio of the pressure drop in the sand to that across the coating, namely,

$$\frac{p_S - p_0}{p_C - p_S} \leqslant \frac{1}{\pi}\frac{\kappa_C l_C}{\kappa_S d_C}\ln\left(\frac{4\kappa_S p_0}{\varphi_S\mu_G u l_C}\right), \tag{3.9}$$

where we have assumed that the overall pressure drop from the metal to the sand is small compared with the absolute pressure in the sand at infinity. For the typical sand and coating properties listed in Table 2, a filling speed of 1 cm/s, and $l_C < 1$ cm of exposed coating, (3.9) gives

$$\frac{p_S - p_0}{p_C - p_S} \leqslant 0.04. \tag{3.10}$$

Hence the error in neglecting the diffusion resistance of the sand is less than 4%. If we further consider that a significant fraction of the polymer vapor condenses soon after it enters the sand, as reported by Fu et al. [22], the error is even less. This result is supported by Sands and Shivkumar [23], who found that varying sand fineness in the range AFS 20-80 had no effect on filling speed in foam strips. Note from (3.9), however, that the error is proportional to the coating permeability. In iron casting, where the coating permeability is more than ten times higher than for aluminum, the pressure drop in the sand is no longer negligible.

If we neglect the diffusive resistance of the sand, then $p_S = p_0$ and (3.1) becomes

$$v_G = \frac{\kappa_C}{\mu_G d_C}\frac{p_M^2 - p_0^2}{2p_M}, \tag{3.11}$$

where we have set $p_C = p_M$ since the viscous resistance of the foam has been neglected. Eq. (3.11) determines how fast gas diffuses through the coating. How much gas escapes in any given time depends on how much of the coating is exposed to gas diffusion.

3.3. A simple model for the escaping gas

Perhaps the simplest model for describing how gas escapes from the decomposition layer is illustrated in Fig. 9. This picture, or one very much like it, has been reproduced by nearly every author over nearly four decades of research in lost foam casting [6,9,10,19,24–26]. The basic assumption is that gas escapes from the mold cavity through a length of exposed coating equal to the separation between the liquid metal and the unmelted foam. In other words, $l_C = l_D$. To balance the mass in the decomposition layer, the filling speed u and thickness l_D adjust in opposite directions (since their product, according to the heat conduction solution of the previous section, must stay approximately constant) until gas is generated in the decomposition layer at the same rate as it escapes. When the metal pressure rises, more gas escapes through the coating, causing l_D to decrease and u to increase. Qualitatively, this trend is certainly consistent with experience: filling speeds do increase with metal pressure. The problem comes in calculating the actual speeds.

Suppose we assume that the liquid foam remains homogeneous until it reaches the coating, where the gas separates from the liquid. The gas diffuses through the coating and into the sand while the liquid, which remains inside the cavity, is eventually overtaken by the advancing liquid metal. In this case, a simple mass balance over the decomposition layer yields

$$2\rho_D l_D v_G = \rho_P u d, \tag{3.12}$$

where d is the thickness of the pattern. Together with the heat conduction analysis of the previous section, (3.11) and (3.12) determine the filling speed u and the thickness of the decomposition layer l_D.

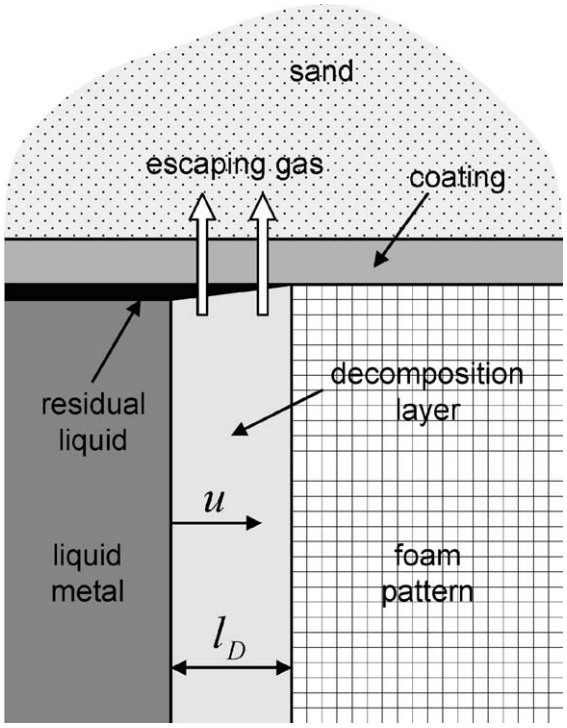

Fig. 9. A simple model for gas escaping from the decomposition layer.

As reasonable as it may seem, it turns out that (3.12) leads to unacceptable quantitative results, and this by such a wide margin that even with a modest allowance for uncertainty in material properties, the discrepancies are inescapable. Littleton et al. [27] were the first to raise concern over the inability of the simple model in Fig. 9 to eliminate all the gas generated at normal filling speeds. To see the consequence of (3.12) in the context of the present model, we use the foam properties in Table 1 together with coating properties from Table 2. Then for specified values of pressure, metal temperature, and pattern thickness, we can solve the seven Eqs. (2.3), (2.4), (2.15)–(2.17), (3.11) and (3.12) for the seven unknowns x_V, l_D, ρ_D, θ_D, λ_D, v_G, and u.

Fig. 10 shows the results for filling speed as a function of metal pressure (measured in meters of aluminum) for a metal temperature of 650 °C and four different values of pattern thickness. There are at least two problems with these results. First, the predicted filling speeds are too slow by an order of magnitude. In aluminum casting, filling speeds are typically 1–2 cm/s. To expose enough coating surface for the gas to escape according to (3.12), the decomposition layer has to widen to the point where heat conduction cannot support the observed filling speeds. Second, according to these results

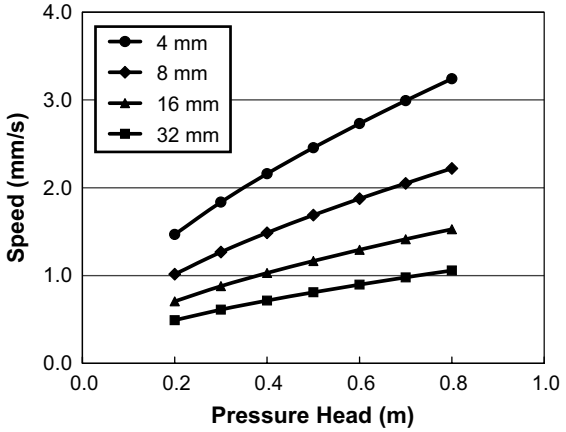

Fig. 10. Filling speed as a function of metal pressure (in meters of aluminum) for a metal temperature of 650 °C and four different values of section thickness, based on the simple model in Fig. 9.

filling speed is strongly affected by section thickness, with thicker sections filling considerably slower than thinner ones. This result follows directly from the mass balance (3.12). As long as λ_D is roughly constant, then (2.15) and (3.12) together imply that $u^2 d$ is also approximately constant. This inverse square-root dependence of filling speed on thickness is clearly evident in Fig. 10. This conclusion, however, is contrary to experimental results reported by Miller [28] that show little or no dependence of filling speed on pattern thickness.

It is clear, then, that the simple model in Fig. 9 is inadequate. To understand what is wrong, we must take a closer look at the special way that foam decomposes near the coating.

4. The coating undercut

4.1. Motivation

In lost foam casting, the liquid metal replaces the volume originally occupied by the foam pattern only after the material in the pattern breaks down and the gas and liquid products move out of the way. Since most foam materials are about 97% air by volume, air is the major substance impeding the forward movement of the liquid metal. But the air by itself would do a poor job of restraining the metal if it were not contained in the honeycombed cellular structure of the individual foam beads that are fused together in the molding process to make the pattern. Until the polymer itself becomes liquid, the closed cells in the foam keep the air from escaping through the coating and into the surrounding sand. As soon as the polymer melts, the air in these cells is free to flow to and through the coating, seeking the lower pressure in the sand. As long as the only path to the coating is through the decomposition layer, though, this motion cannot occur without an additional expenditure of energy above that required simply to melt the foam. The decomposition layer is bounded on one side by liquid metal several hundred degrees hotter than the melting temperature of the foam, and so the average temperature of the material in the decomposition layer must rise well above the melting temperature of the polymer, which causes a significant fraction of the polymer liquid to degrade and vaporize before it ever gets to the coating. These three components of the pattern decomposition energy (melting, heating, and polymer degradation/vaporization) are each expressed by one of the three terms in (2.19). Using the properties of polystyrene foam listed in Table 1 together with the temperature solution in Section 2, it is easy to show that the energy ε_P required just to melt the foam represents less than 20% of the total energy required to remove the pattern from the path of the liquid metal.

If there were another way for the air in the foam to reach the coating without first entering the decomposition layer, the decomposition energy would be much lower. For example, if the pattern has a high inter-bead porosity, some or all of the air can reach the coating by diffusing between the beads in the unmelted pattern and escaping through the coating ahead of the metal front [26,27]. In this case, the beads nearest the metal simply collapse upon melting, the air they contain diffuses through the permeable pattern structure, and the small volume of polymer liquid that remains is simply swept aside. Although such rapid foam collapse is usually undesirable, it can be prevented for the most part by careful molding of the foam pattern. But even in cases when the molded foam is sound enough to prevent such a collapse, something very much like it can still occur in the foam cells immediately adjacent to the coating.

Consider the schematic illustration in Fig. 11. When the polymer cells melt in the interior of the pattern, their contents must enter the decomposition layer and flow parallel to the liquid metal before the gas can escape through the coating. But on the boundary of the pattern, a melting foam cell is able to expel its air directly into the coating without any need for it to enter the decomposition layer. The coating presents almost no diffusion resistance to the small quantity of air that escapes when a single boundary cell collapses. After one boundary cell collapses, liquid foam from the decomposition layer fills the resulting void, heating the next cell, and causing it to collapse as well. This process continues until a narrow *undercut* forms between the unmelted foam and the coating. The length of this undercut, which determines how much of the coating is exposed to gas diffusion, is controlled by a balance between the heat flux into the foam

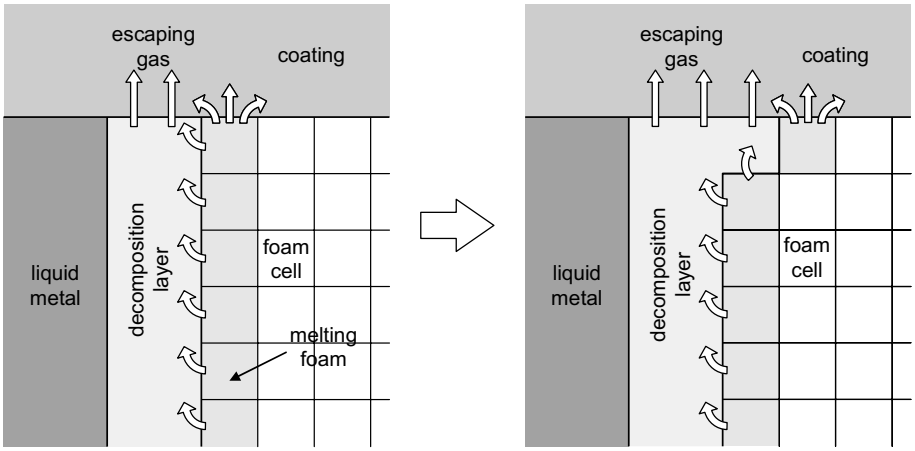

Fig. 11. Schematic illustration of foam collapse in the cells adjacent to the coating, leading to the formation of the undercut.

and the rate of energy expended in collapsing the foam at its leading edge.

To our knowledge, the concept of a coating undercut is an entirely new proposition in lost foam casting. While conditions certainly exist to support its formation and there appears to be scattered experimental evidence to confirm its existence, for the time being we must regard it only as a reasonable hypothesis. In keeping with this level of uncertainty, therefore, we propose a relatively basic model for the undercut that does not extend beyond our current level of understanding.

4.2. Energy balance

Consider steady mold filling with the idealized undercut geometry illustrated in Fig. 12. Position the origin of coordinates at the leading edge of the undercut with the x-axis pointing in the opposite direction of flow. Let l_C measure the length of the undercut from its leading edge back to the surface of the liquid metal. Relative to these coordinates, both the coating and the pattern move with positive velocity u. We assume that the liquid foam enters the undercut at $x = l_C$ with the same composition and average temperature as in the decomposition layer. As the liquid foam moves down the undercut, it loses gas through the coating on one side and sheds liquid on the other as it shears against the unmelted foam. For simplicity, we assume these two losses occur in the same proportion, so that the composition of the remaining liquid foam is unchanged. And we assume that the lateral heat convection created by both mass fluxes is sufficient to keep the main gas/liquid mixture from cooling by lateral conduction to either the coating or the foam. The gas loses heat to the coating as it diffuses through it on one side of the undercut and the rejected liquid first heats and then melts some of the foam on the other. As the foam melts along the undercut, the undercut

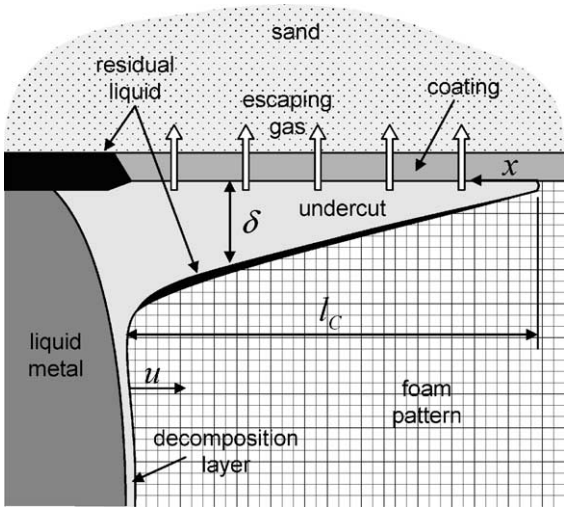

Fig. 12. Idealized geometry of the proposed coating undercut.

widens with increasing x and the amount of liquid accumulated on the foam increases as well. Polymer liquid does not deposit on the inside of the coating along the undercut because the coating is not yet warm enough for the liquid to wet its surface [29].

Let $\theta(x)$ denote the temperature of the liquid foam in the undercut and $\delta(x)$ its width. Further, let $\delta_D = \delta(l_C)$ denote the width of the undercut at the point where it joins the decomposition layer. The convection of energy into the undercut from the decomposition layer is given by

$$\rho_P u \varepsilon_D (d/2 - \delta_D), \tag{4.1}$$

where d represents the pattern thickness, as before. If we assume that gas escapes through the coating uniformly along the undercut, then the convection of energy down the undercut decreases linearly with x.

As gas escapes through the coating, it removes energy from the undercut. The energy removed per unit length is given by

$$\frac{u}{l_C}(d/2-\delta_D)x_V\rho_F\varepsilon_V+\frac{ud}{2l_C}\varphi\rho_A^0\varepsilon_A. \tag{4.2}$$

The corresponding energy per unit length lost as the liquid deposits on the foam is

$$\frac{u}{l_C}(d/2-\delta_D)(1-x_V)\rho_F\varepsilon_L. \tag{4.3}$$

From (4.1)–(4.3), the energy balance in the undercut may be expressed as

$$\begin{aligned}&k_D\frac{\partial}{\partial x}\left(\delta\frac{\partial\theta}{\partial x}\right)+\frac{\partial}{\partial x}\left[\frac{x}{l_C}(d/2-\delta_D)\rho_P u\varepsilon_D\right]\\&\quad-\frac{u}{l_C}(d/2-\delta_D)\rho_F[x_V\varepsilon_V+(1-x_V)\varepsilon_L]\\&\quad-\frac{ud}{2l_C}\varphi\rho_A^0\varepsilon_A=0.\end{aligned} \tag{4.4}$$

With the help of (2.8) and (2.9), this simplifies to

$$\begin{aligned}&k_D\frac{\partial}{\partial x}\left(\delta\frac{\partial\theta}{\partial x}\right)+\frac{x}{l_C}(d/2-\delta_D)\rho_P c_D u\frac{\partial\theta}{\partial x}\\&\quad-\frac{u}{l_C}\delta_D\varphi\rho_A^0\varepsilon_A=0.\end{aligned} \tag{4.5}$$

To solve this equation, we need to supply an expression for $\delta(x)$, which must come from a separate energy balance for the residual liquid that deposits on the foam.

Let $\delta_L(x)$ denote the thickness of residual liquid that accumulates between the pattern and the undercut. It is made up of liquid rejected from the undercut as well as additional liquid created as the foam melts and the undercut widens. From the above assumptions, we have

$$\delta_L(x)=(1-\varphi)\left[(d/2-\delta_D)(1-x_V)\frac{x}{l_C}+\delta-\delta(0)\right]. \tag{4.6}$$

The first term in the brackets represents the liquid rejected from the undercut. The last two represent the additional liquid created by melting the foam. Now let $\theta_L(x)$ denote the average temperature of the residual liquid at the point x. Then if we neglect longitudinal conduction (the liquid is probably not smoothly connected anyway) and use (4.3), the energy balance in the residual liquid may be expressed as

$$\frac{u}{l_C}(d/2-\delta_D)(1-x_V)\rho_F\varepsilon_L(\theta)=\rho_S u\frac{\partial}{\partial x}[\delta_L\varepsilon_L(\theta_L)]. \tag{4.7}$$

For simplicity, we have taken the densities of the liquid and solid polymer to be equal. With (4.6), this equation reduces to

$$\begin{aligned}&(d/2-\delta_D)(1-x_V)c_L(\theta-\theta_L)\frac{1}{l_C}\\&\quad=\varepsilon_L(\theta_L)\frac{\partial\delta}{\partial x}+\frac{\delta_L c_L}{(1-\varphi)}\frac{\partial\theta_L}{\partial x}.\end{aligned} \tag{4.8}$$

Suppose again for simplicity we set

$$\theta_L=\frac{1}{2}(\theta+\theta_P). \tag{4.9}$$

Then (4.8) becomes

$$\begin{aligned}&(d/2-\delta_D)(1-x_V)(\theta-\theta_P)\frac{1}{l_C}\\&\quad=2\frac{\varepsilon_L(\theta_L)}{c_L}\frac{\partial\delta}{\partial x}+\frac{\delta_L}{(1-\varphi)}\frac{\partial\theta}{\partial x}.\end{aligned} \tag{4.10}$$

The temperature boundary conditions in the undercut are

$$\theta(0)=\theta_P,\quad \theta(l_C)=\theta_D. \tag{4.11}$$

Since the foam cannot collapse on a scale smaller than the size of an individual foam cell, we assume that the undercut narrows to the nominal cell size δ_0 of the foam at $x=0$. The heat flux at this point must be sufficient to sustain a rate of foam collapse equal to the filling speed. These two conditions are expressed by

$$\delta(0)=\delta_0,\quad k_D\frac{\partial\theta}{\partial x}(0)=u\rho_B\varepsilon_C, \tag{4.12}$$

where ε_C is the collapse energy of the foam pattern per unit mass and ρ_B is the boundary density of the pattern. Here a distinct surface density is introduced for the foam since the density of molded foam is usually higher near the boundary [30]. Even though in general the collapse energy ε_C of the foam is smaller than its melting energy ε_P, we still assume that the corresponding temperatures are approximately the same.

4.3. Solving the energy balance equations

Before we solve the coupled, nonlinear differential equations (4.5) and (4.10) subject to the boundary conditions (4.11) and (4.12), it is convenient first to introduce the following set of nondimensional variables:

$$\begin{aligned}&\hat{x}=x/l_C,\quad \hat{\delta}=2\delta/d,\quad \hat{\delta}_L=2\delta_L/d,\\&\hat{\theta}=c_D(\theta-\theta_P)/\varepsilon_P.\end{aligned} \tag{4.13}$$

In terms of these variables, (4.5) and (4.10) may be written as

$$(\hat{\delta}\hat{\theta}')'+P\hat{x}(1-\hat{\delta}_D)\hat{\theta}'-P\hat{\delta}_D\varphi\frac{\rho_A^0\varepsilon_A}{\rho_P\varepsilon_P}=0, \tag{4.14}$$

$$(1-\hat{\delta}_D)(1-x_V)\hat{\theta}=\hat{\delta}'(\hat{\theta}+2)+\frac{\hat{\delta}_L\hat{\theta}'}{1-\varphi}, \tag{4.15}$$

where a prime denotes $\partial/\partial\hat{x}$ and

$$P = \frac{\rho_P c_D u l_C}{k_D}. \tag{4.16}$$

From (4.11)–(4.13) and (4.16) the corresponding nondimensional boundary conditions are

$$\hat{\theta}(0) = 0, \quad \hat{\theta}(1) = \hat{\theta}_D, \quad \hat{\delta}(0) = \hat{\delta}_0,$$
$$\hat{\theta}'(0) = P\frac{\rho_B \varepsilon_C}{\rho_P \varepsilon_P}. \tag{4.17}$$

In principle, (4.14) and (4.15) may be solved by numerical integration, starting from $\hat{x} = 0$ and iterating on the choice of u and $\hat{\delta}_D$ until the computed solution at $\hat{x} = 1$ matches the prescribed values of $\hat{\theta}$ and $\hat{\delta}$.

The darker lines in Fig. 13 graph the solution of (4.14) and (4.15) for the foam properties listed in Table 1 and the representative values $x_V = 0.3$ and $P = 100$. The temperature $\hat{\theta}$ stays virtually uniform over the entire length of the undercut, except very near $x = 0$, where it drops precipitously to the melting temperature of the foam. This is a result of strong longitudinal convection together with the assumption of negligible lateral conduction losses. The undercut width is very nearly linear in $\hat{x}$, except near $\hat{x} = 0$, where it must level off to a zero slope to be compatible with (4.15) and the boundary conditions in (4.17).

It turns out that over a wide range of material and process parameters, the solution to the coupled, nonlinear system (4.14) and (4.15) may be approximated quite well by the solution to the decoupled, linear system

$$\hat{\delta}_0\hat{\theta}'' + P\hat{x}(1-\hat{\delta}_D)\hat{\theta}' = 0, \tag{4.18}$$
$$(1-\hat{\delta}_D)(1-x_V)\hat{\theta}_D = \hat{\delta}'(\hat{\theta}_D + 2). \tag{4.19}$$

The solution of (4.19) is

$$\hat{\delta}(x) = \hat{\delta}_0 + (\hat{\delta}_D - \hat{\delta}_0)\hat{x}, \tag{4.20}$$

where

$$\hat{\delta}_D = \frac{(1-x_V)\hat{\theta}_D + \hat{\delta}_0(\hat{\theta}_D + 2)}{(2-x_V)\hat{\theta}_D + 2}. \tag{4.21}$$

The solution of (4.18) is

$$\hat{\theta} = \frac{\operatorname{erf}(\lambda_U \hat{x})}{\operatorname{erf}(\lambda_U)}\hat{\theta}_D, \tag{4.22}$$

where

$$\lambda_U^2 = \frac{1-\hat{\delta}_D}{2\hat{\delta}_0}P = \frac{d/2-\delta_D}{\delta_0}\frac{\rho_P c_D u l_C}{2k_D}. \tag{4.23}$$

The solution (4.20) and (4.22) is shown by the lighter lines in Fig. 13. Very little accuracy is lost in the approximation. For simplicity in what follows, we use only the approximate solution.

Combining (4.17) and (4.22), we obtain

$$\hat{\theta}'(0) = \frac{\rho_P c_D u l_C}{k_D}\frac{\rho_B \varepsilon_C}{\rho_P \varepsilon_P} = \frac{2}{\sqrt{\pi}}\frac{\lambda_U}{\operatorname{erf}(\lambda_U)}\hat{\theta}_D. \tag{4.24}$$

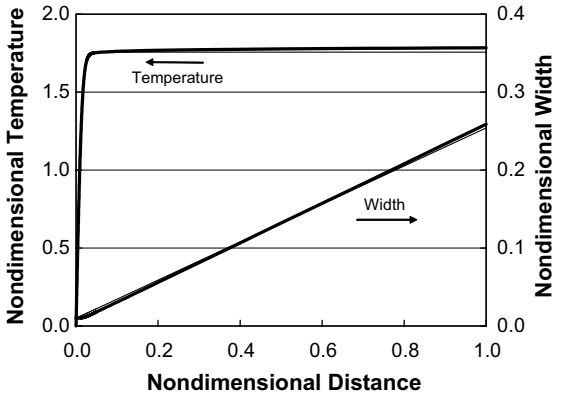

Fig. 13. Nondimensional undercut temperature and width as a function of distance from the leading edge. The heavy lines represent the numerical solution of the coupled, nonlinear equations (4.14) and (4.15) for representative values $x_V = 0.3$ and $P = 100$, while the lighter lines represent the corresponding solution of the approximate equations (4.18) and (4.19).

Since λ_U is usually large enough to make the approximation $\operatorname{erf}(\lambda_U) = 1$, (4.24) may be expressed as

$$u = \frac{k_D\hat{\theta}_D}{\rho_B c_D}\frac{\varepsilon_P}{\varepsilon_C}\sqrt{\frac{2(d/2-\delta_D)\rho_P c_D u}{\pi k_D \delta_0 l_C}}. \tag{4.25}$$

This is very nearly the desired result. All that remains is to derive an expression for the undercut length l_C. For that we need to consider a mass balance for the escaping gas.

4.4. Mass balance

Let ρ_G denote the density of the gas in the undercut. Then if we require that all the gas generated in the decomposition layer escape through the length of coating exposed by the undercut, we have

$$\frac{1}{2}du\varphi\rho_A^0 + (d/2-\delta_D)ux_V\rho_F = \rho_G v_G l_C, \tag{4.26}$$

where v_G is given by (3.11) and from the ideal gas law

$$\rho_G = \frac{\varphi\rho_A^0 + x_V\rho_F}{\varphi\dfrac{p_0\theta}{p_M\theta_0} + x_V\rho_F\dfrac{R\theta}{p_M M_V}}. \tag{4.27}$$

We neglect all viscous losses in the undercut compared with the pressure drop across the coating and assume that the pressure in the undercut is uniform and equal to p_M. The gas temperature in the undercut is nearly uniform until just before $x = 0$, and so we assume that ρ_G is approximately constant and given by (4.27) with $\theta = \theta_D$. Since the volume fraction of liquid in the decomposition layer/undercut is even less than the tiny solid fraction in the original foam, it is a very good approximation to neglect the first term in the denominator of (2.4). Then with (4.27) we have, approximately,

$$\frac{\rho_D}{\rho_P} = \frac{\rho_G}{\varphi\rho_A^0 + x_V\rho_F}. \tag{4.28}$$

Since the amount of air released by the formation of the undercut is small compared with the total amount of air and vapor coming from the rest of the pattern,

$$\varphi\rho_A^0\delta_D \ll (x_V\rho_F + \varphi\rho_A^0)(d/2 - \delta_D) \tag{4.29}$$

and (4.26) becomes, approximately,

$$(d/2 - \delta_D)u\rho_P = \rho_D v_G l_C, \tag{4.30}$$

where we have also used (4.28). Finally, Eqs. (4.30) and (4.25) combine to yield

$$u = \frac{1}{\rho_B\varepsilon_C}\sqrt{\frac{2\rho_D c_D k_D v_G}{\pi\delta_0}}(\theta_D - \theta_P). \tag{4.31}$$

The entire solution for the filling speed u, gas fraction x_V, average temperature θ_D, average density ρ_D, average specific heat c_D, and filter velocity v_G follows from the simultaneous solution of (2.3), (2.9), (2.16), (2.17), (3.11) and (4.31).

So far nothing has been said about the fate of the residual liquid that collects along the inside of the undercut. According to (4.6), the amount of this liquid increases as the foam approaches the surface of the liquid metal. While the details of the juncture between the decomposition layer and the undercut are still unclear, it is likely that broken sections of this liquid are swept towards the coating by the liquid foam rushing out of the decomposition layer. The coating should readily absorb the liquid (Fig. 12) as long as the escaping gas ahead of this point has heated the coating sufficiently for it to wet the polymer liquid [29]. The analysis of heat transfer from the gas to the coating is relatively straightforward and we do not consider it further here.

5. Filling results

5.1. Qualitative trends

Three important qualitative observations can now be made based on the results derived so far. First note from (4.31) that *the filling speed is independent of the section thickness*. Although somewhat contrary to intuition, this conclusion is confirmed by Miller [28], as well as a growing body of mold filling data from more recent real-time X-ray experiments at General Motors. Ordinarily, one would expect the lower surface-area-to-volume ratio in thicker parts to impede the elimination of decomposition products from the mold cavity, leading to lower filling speeds. The reason that this does not happen is because the undercut lengthens with part thickness, allowing it to accommodate a greater volume of escaping gas.

The second observation is that according to (4.31) the filling speed u is inversely proportional to the pattern collapse energy ε_C. Suppose we assume that the foam collapses at the temperature θ_C and that its collapse energy is given by

$$\rho_P\varepsilon_C = (\varphi\rho_A^0 c_A + \rho_F c_S)(\theta_C - \theta_0). \tag{5.1}$$

Polystyrene foam collapses at about 120 °C [11], less than 100° above the initial pattern temperature, which should be equal to the sand temperature by the time the casting is poured. If the sand temperature rises just 10°, the collapse energy drops by more than 10%. It follows that *filling speed is sensitive to even small changes in sand temperature*. This result, too, seems to contradict intuition. According to (2.19), raising the sand temperature as much as 30 °C reduces the decomposition energy (2.19) by only 5%. Yet when Buesch et al. [31] raised the sand temperature from 26 to 60 °C, they observed filling speeds increase by about 50%. The present model predicts the same thing.

The third observation is that, according to (4.31), filling speed is inversely proportional to the surface density of the foam. The foam molding process usually produces a higher density near the pattern boundary where the beads are in direct contact with the hot mold surface. Typically, the pattern's boundary density is about twice as large as its nominal density [30]. Patterns cut from board stock, on the other hand, would not have this higher-density outer skin. Consequently, *filling speeds in cut foam should be significantly higher than in molded foam.* Again, this result is borne out by experiments. Liu et al. [32] measured filling speeds in cut foam that were almost double those in molded foam. Bennett et al. [33] made a similar observation. Until now, no one has offered a plausible explanation for these results.

All three of these results depend on the existence of the coating undercut, and none has ever been explained before. But these are just qualitative trends. The real test of the model is how well it predicts actual filling speeds.

5.2. Filling speeds

To calculate filling speeds with the undercut model, we need to specify two more properties of the foam: the boundary density ρ_B and the nominal cell size δ_0. Strictly speaking, both are determined more by the foam molding process than they are by the properties of the bead itself. Cell size depends on the amount of bead expansion and the boundary density on parameters of the molding steam cycle. For purposes of this paper, we assume a boundary density twice as large as the nominal density of the foam and a cell size of 50 μm (Table 1).

Fig. 14 displays the calculated filling speed for a polystyrene pattern as a function of pressure (measured in meters of aluminum) at a metal surface temperature of

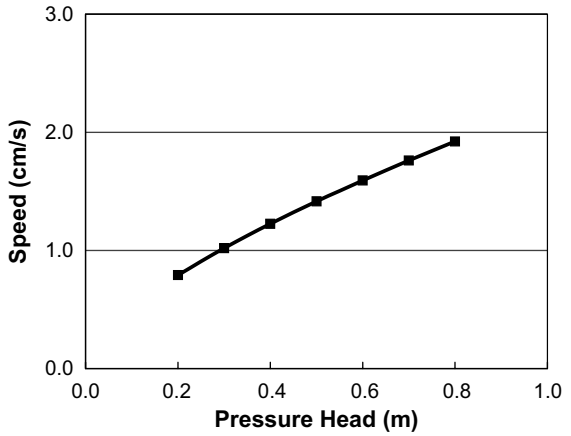

Fig. 14. Filling speed as a function of metal pressure (in meters of aluminum) for a polystyrene foam and a metal temperature of 650 °C, based on the undercut model illustrated in Fig. 12.

650 °C, using the material properties listed in Tables 1 and 2. The calculated speeds are now in line with experience. Most recent studies involving mica-based coatings on molded foam report filling speeds in the 1–2 cm/s range [33–35]. Filling speed increases with pressure as expected, but slightly faster than the square root dependence indicated in (4.31) because ρ_D is not constant. Less gas is generated at faster filling speeds (Fig. 2), which increases the liquid foam density ρ_D at the same time that higher pressures increase the gas velocity v_G through the coating.

Perhaps more interesting is the dependence of filling speed on metal temperature, shown in Fig. 15 for a constant aluminum head of 0.5 m. It turns out that metal temperature has almost no effect on filling speed. Even though higher metal temperatures increase the heat flux into the foam, they also generate more gas and the two trends very nearly balance each other out. Many experimenters have reported little or no dependence of filling speed on metal temperature [10,31,36,37], consistent with these results.

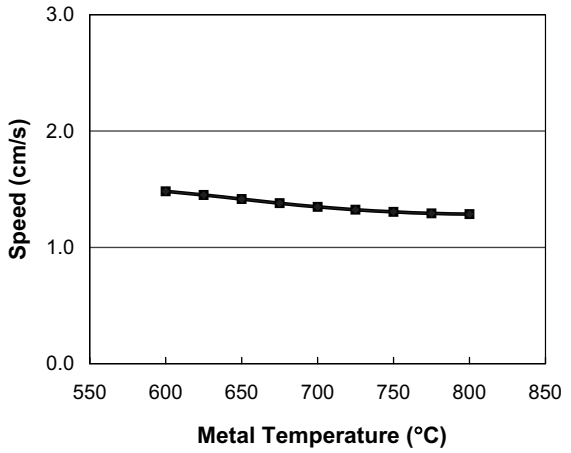

Fig. 15. Filling speed as a function of metal temperature for a polystyrene foam and a metal pressure corresponding to 0.5 m of aluminum, based on the undercut model illustrated in Fig. 12.

5.3. Undercut dimensions

Besides the encouraging behavioral inferences from the model, we cannot cite any published accounts where a coating undercut has been detected explicitly. Nevertheless, it is still important that the length and breadth of the undercut fall within reasonable bounds for the model to be plausible. Figs. 16 and 17 plot the

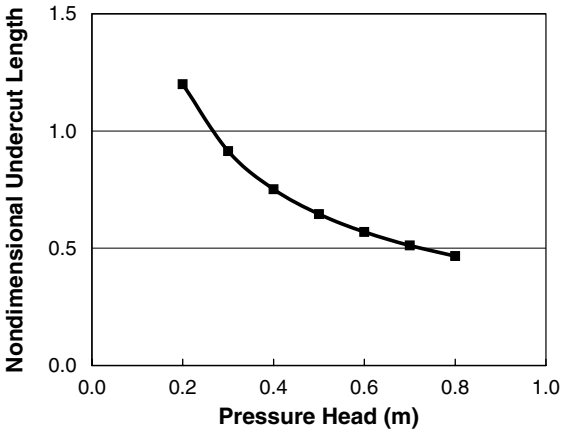

Fig. 16. Nondimensional undercut length as a function of metal pressure (in meters of aluminum) for a polystyrene foam and a metal temperature of 650 °C.

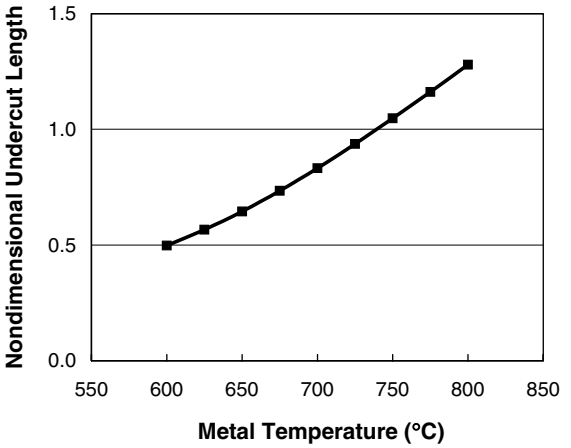

Fig. 17. Nondimensional undercut length as a function of metal temperature for a polystyrene foam and a metal pressure corresponding to 0.5 m of aluminum.

nondimensional undercut length $2l_C/d$ in polystyrene foam as a function of metal pressure and temperature, respectively. The length of the undercut is equal to roughly half the thickness of the part. It decreases with pressure and lengthens with increasing metal temperature.

The maximum width of the undercut varies to a less significant degree, penetrating about 15% of the part thickness from each side. This dimension, about 1 mm in typical parts, is much larger than the thickness of the decomposition layer and should be readily detectable with appropriate instrumentation. At these widths, any viscous pressure losses down the length of the undercut should be negligible, which justifies our assumption of a uniform filter velocity v_G along the undercut.

6. Discussion

This paper presents a mathematical model of foam ablation for lost foam casting of aluminum that correctly accounts for many experimental observations that up to now have had no satisfactory explanation. Governing equations are developed for heat conduction and polymer vaporization in the narrow *decomposition layer* between the liquid metal and the foam pattern, and for the flow of foam decomposition products through a proposed *coating undercut* at the pattern boundary where gas diffuses through the coating and into the sand.

It has been generally accepted for nearly four decades now that the gas generated by the decomposing pattern escapes through a length of exposed coating approximately equal to the separation between the liquid metal and the unmelted foam. Recent foam pyrolysis data [12,14], however, has allowed us to test that hypothesis here for the first time, resulting in predicted filling speeds a full order of magnitude smaller than measured values. Furthermore, it leads to a strong dependence of filling speed on pattern thickness—with thicker parts filling considerably slower than thinner ones—something that is also not observed in experiments.

The entirely new model for gas evacuation proposed in this paper is based on a reasonable hypothesis for the unique way that foam cells decompose along the boundary of the pattern. Not only does this model predict correct filling speeds for a polystyrene pattern coated with a mica-based refractory, but it also accounts for a number of seemingly counterintuitive experimental observations that have never been explained before: filling speeds are independent of pattern thickness, strongly dependent on sand temperature, weakly dependent on metal temperature, and much faster in cut foam compared with molded foam.

Although ablation is only one means by which foam decomposes in lost foam casting, it is perhaps the most important mechanism. The present model is a key ingredient in an analysis of metal filling in lost foam casting of aluminum, an important step towards understanding the ways that foam decomposition can contribute to fill related casting defects.

Acknowledgements

The authors would like to extend their thanks to Taras Molibog, a former Ph.D. student at the University of Alabama at Birmingham, for sharing preliminary data from his foam pyrolysis experiments and for many useful and stimulating discussions on foam decomposition. We are also indebted to David Goettsch and Jerry Barendreght of General Motors Powertrain Group for their valuable work in real-time X-ray imaging of mold filling.

References

[1] T.R. Smith, Method of Casting, US Patent No. 3,157,924, 1964.
[2] J.R. Brown, The lost foam casting process, Met. Mater. 8 (1992) 550–555.
[3] Q. Zhao, T.W. Gustafson, M. Hoover, M.C. Flemings, Fold formation in the lost foam aluminum process, in: S.K. Das (Ed.), Aluminum 2003, TMS, Warrendale, 2003, pp. 121–132.
[4] H.L. Tsai, T.S. Chen, Modeling of evaporative pattern process, Part I: Metal flow and heat transfer during the filling stage, AFS Trans. 96 (1988) 881–890.
[5] C.W. Hirt, M.R. Barkhudarov, Lost foam casting simulation with defect prediction, in: B.G. Thomas, C. Beckermann (Eds.), Modeling of Welding, Casting and Advanced Solidification Processes VIII, TMS, Warrendale, 1998, pp. 51–57.
[6] Y. Liu, S.I. Bakhtiyarov, R.A. Overfelt, Numerical modeling and experimental verification of mold filling and evolved gas pressure in lost foam casting, J. Mater. Sci. 37 (2002) 2997–3003.
[7] C.M. Wang, A.J. Paul, W.W. Fincher, O.J. Huey, Computational fluid flow and heat transfer during the EPC process, AFS Trans. 101 (1993) 897–904.
[8] O. Gurdogan, H. Huang, H.U. Akay, W.W. Fincher, V.E. Wilson, Mold-filling analysis for ductile iron lost foam castings, AFS Trans. 104 (1996) 451–459.
[9] S. Shivkumar, Modelling of temperature losses in liquid metal during casting formation in expendable pattern casting process, Mater. Sci. Technol. 10 (1994) 986–992.
[10] X. Liu, C.W. Ramsay, D.R. Askeland, Study on mold filling control mechanisms in the EPC process, AFS Trans. 102 (1994) 903–914.
[11] S. Mehta, S. Biederman, S. Shivkumar, Thermal degradation of foamed polystyrene, J. Mater. Sci. 30 (1995) 2944–2949.
[12] T.V. Molibog, H. Littleton, Experimental simulation of pattern degradation in lost foam, AFS Trans. 109 (2001) 1523–1554.
[13] D. Weaire, S. Hutzler, The Physics of Foams, Oxford University Press, New York, 1999, pp. 6–8.

[14] T.V. Molibog, H. Littleton, Degradation of expanded polystyrene patterns, AFS Trans. 110 (2002) 1483–1496.
[15] C.H.E. Tseng, D.R. Askeland, Thermal and chemical analysis of the foam, Refractory coating and sand in the EPC process, AFS Trans. 100 (1992) 509–518.
[16] M. Sands, S. Shivkumar, EPS molecular weight and foam density effects in the lost foam process, J. Mater. Sci. 38 (2003) 2233–2239.
[17] R.D. Butler, R.J. Pope, Some factors involved in full mould casting with unbonded sand moulds, Brit. Foundryman 4 (1964) 178–191.
[18] C.-H. Tseng, D.R. Askeland, A study of selected process parameters for the evaporative pattern casting process, AFS Trans. 99 (1991) 455–464.
[19] R.P. Walling, J.A. Dantzig, Mechanisms if mold filling in the EPC process, AFS Trans. 102 (1994) 849–854.
[20] A.E. Scheidegger, The Physics of Flow through Porous Media, third ed., University of Toronto Press, Toronto, 1974, pp. 102–107.
[21] H.S. Carslaw, J.C. Jaeger, Conduction of Heat in Solids, second ed., Clarendon Press, Oxford, 1959, p. 269.
[22] J. Fu, H.L. Tsai, D.R. Askeland, Transport of foam decomposition products into the sand in the lost foam casting process, AFS Trans. 104 (1996) 263–270.
[23] M. Sands, S. Shivkumar, Influence of coating thickness and sand fineness on mold filling in the lost foam casting process, J. Mater. Sci. 38 (2003) 667–673.
[24] H.B. Dieter, A.J. Paoli, Sand without binder for making full mold castings, AFS Trans. 75 (1967) 147–160.
[25] M.H. Warner, B.A. Miller, H.E. Littleton, Pattern pyrolysis defect reduction in lost foam castings, AFS Trans. 106 (1998) 777–785.
[26] J. Rossacci, S. Shivkumar, Influence of EPS bead fusion on pattern degradation and casting formation in the lost foam process, J. Mater. Sci. 38 (2003) 2321–2330.
[27] H.E. Littleton, T. Molibog, W. Sun, The role of pattern permeability in lost foam casting, AFS Trans. 111 (2003) 1265–1277.
[28] B.A. Miller, Pattern pyrolysis defect reduction in lost foam castings, Masters Thesis, University of Alabama, Birmingham, Alabama, 1996.
[29] Y. Sun, H.L. Tsai, D.R. Askeland, Investigation of wetting and wicking properties of refractory coating in the EPC process, AFS Trans. 100 (1992) 297–308.
[30] M. Hill, A.E. Vrieze, T.L. Moody, C.W. Ramsay, D.R. Askeland, Effect of metal velocity on defect formation in Al LFCs, AFS Trans. 106 (1998) 365–374.
[31] A. Buesch, C. Carney, T. Moody, C. Wang, C.W. Ramsay, D.R. Askeland, Influence of sand temperature on formation of pyrolysis defects in aluminum lost foam castings, AFS Trans. 108 (2000) 615–621.
[32] J. Liu, C.W. Ramsey, D.R. Askeland, Effects of foam density and density gradients on metal fill in the LFC process, AFS Trans. 105 (1997) 435–442.
[33] S. Bennett, T. Moody, A. Vrieze, M. Jackson, D.R. Askeland, C.W. Ramsay, Pyrolysis defects in aluminum lost foam casting, AFS Trans. 107 (1999) 795–803.
[34] W.L. Sun, H.E. Littleton, C.E. Bates, Real-time X-ray investigations on lost foam mold filling, AFS Trans. 110 (2002) 1347–1356.
[35] E.N. Pan, G.L. Sheu, The filling phenomena of lost foam cast irons and aluminum alloys, AFS Trans. 111 (2003) 1255–1263.
[36] S. Shivkumar, Casting characteristics of aluminum alloys in the EPC process, AFS Trans. 101 (1993) 513–518.
[37] C. Wang, C.W. Ramsay, D.R. Askeland, Processing variable significance on filling thin plates in the LFC process—the staggered, nested factorial experiment, AFS Trans. 105 (1997) 427–434.